Biomass and Bioenergy 180 (2024) 107020

Contents lists available at ScienceDirect

Biomass and Bioenergy

journal homepage: www.elsevier.com/locate/biombioe

Mild production of γ-valerolactone, a biofuel precursor, through the catalytic hydrogenation of a biomass derivative using hydrogen produced by photoelectrochemical water splitting

Adrián García, Elianny Da Silva, María Erans, Ramón Fernández-Domene, Rita Sánchez-Tovar **, Benjamin Solsona *

Department of Chemical Engineering, ETSE, Universitat de València, Av. Universitat s/n, 46100, Burjassot-Valencia, Spain

ARTICLE INFO

Keywords:
Coupled process
Photoelectrocatalysis
γ-valerolactone from levulinic acid
Hydrogen
Water splitting
Biofuel

ABSTRACT

In this article, an efficient and innovative coupled system that involves hydrogen generation from water and hydrogenation of a biomass derived compound is shown for the first time. We have demonstrated that it is possible to use hydrogen produced from photoelectrochemical water splitting for the hydrogenation of a widely available biomass-derived compound (levulinic acid) into a versatile fuel component and/or precursor (γ-valerolactone). This compound, conversely to hydrogen, can be easily stored and handled. The photoelectrocatalyst selected was a TiO_2 nanostructure synthesized by electrochemical anodization. The hydrogen produced was simultaneously used to carry out a hydrogenation reaction to transform levulinic acid into γ-valerolactone. The generated hydrogen was transferred to a catalytic reactor containing an aqueous solution of levulinic acid (LA) in the presence of a Ru based catalyst. Remarkable formation of γ-valerolactone (GVL) was obtained at temperatures as low as 30–60 °C. Yields to GVL of ca. 95 % have been obtained with this novel coupled system at only 60 °C. These results confirm the potential utilization in the biomass valorization of in-situ hydrogen production by photoelectrochemical water splitting.

1. Introduction

Increasing population is one of the causes of massive consumption of fossil sources to produce energy, which has triggered a rise in greenhouse gases emission [1,2]. The use of biomass to produce energy has been used as an alternative in order to obtain energy and also added value chemicals, such as different solvents, important precursors and biofuels [3]. One of these compounds is γ-valerolactone (GVL), which is a versatile chemical platform that can be produced from different biomass feedstocks and has a wide range of applications from production of solvents [4–7], fine chemicals [6–10] and especially fuels [6–9,11,12].

The production of GVL from levulinic acid (LA), a common intermediate derived from biomass, involves a hydrogenation step. Therefore, GVL can be produced from LA if a catalyst and a proper hydrogen source are used [13]. Several hydrogen sources have been used to carry out the reaction, such as formic acid, pressurized hydrogen or alcohols [14–17]. Clean H_2 generation via water splitting could be deployed as a sustainable technology to achieve a decarbonize economy. However, water splitting requires high amount of energy. Photoelectrochemical (PEC) water splitting is one of the most promising green hydrogen production methods [18–20]. It directly uses solar light arriving on a semiconductor to split the water molecule and generate hydrogen and oxygen in separate electrodes, thus avoiding safety concerns and allowing facile separation of both gases. In this process, no large energy inputs are needed, which is one of the main disadvantages of simple water electrolysis. Besides, PEC, unlike other techniques regarded as environmentally friendly, such as solar thermolysis, can be carried out at room temperature. Moreover, PEC cells are very simple to build and to scale-up, requiring minimal auxiliary components. Therefore, although PEC water splitting is still a technology under development and more research is needed, its clear advantages over other hydrogen production methods and the minimum environmental impacts associated, make this technique a very promising one.

* Corresponding author.
** Corresponding author.
E-mail addresses: rita.sanchez@uv.es (R. Sánchez-Tovar), Benjamin.solsona@uv.es (B. Solsona).

https://doi.org/10.1016/j.biombioe.2023.107020
Received 25 July 2023; Received in revised form 20 November 2023; Accepted 27 November 2023
Available online 3 December 2023

For the hydrogenation reaction (LA to GVL) to take place efficiently, typical metal catalysts contain noble metals such as Ru, Pd or Pt [21,22]. Currently, Ru sites are considered as the active site of choice for this reaction. Then, although Ru does not present optimal hydrogenating properties in the gas-phase if compared to Pd or Pt, DFT calculations have demonstrated that this metal is extremely reactive and selective for the hydrogenation of levulinic acid to yield γ-valerolactone if hydrogen is fed using an aqueous media. The oxophilic character of ruthenium has been proposed to be the main responsible for this enhanced performance [22].

TiO_2 has been widely investigated as a photocatalyst, due to its chemical and morphological properties, and low production cost [23,24]. An interesting method to synthesize TiO_2 nanostructures is the electrochemical anodization due to its operational simplicity. When employing this technique, the anodization potential, time, temperature, hydrodynamic conditions and type of electrolyte influence the size, shape and crystallinity of the nanostructure [25,26]. Therefore, by controlling these parameters, compact, porous or sponge-like structures can be produced. For photoelectrocatalytic applications, it has been demonstrated that nanotubular structures, with their perfectly defined and ordered geometry, are very attractive because they allow obtaining a high specific surface area and an improved photocatalytic activity due to the enhanced separation of photogenerated electron-hole pairs, hence reducing recombination losses and increasing the overall process efficiency [27–29].

In this work, hydrogen produced by photoelectrochemical water splitting using TiO_2 is used to transform levulinic acid derived from biomass to produce γ-valerolactone in a catalytic reactor using a ruthenium-based catalyst. This coupled process offers numerous advantages, including the use of renewable energy sources, green production of hydrogen, mild reaction conditions, and an environmentally friendly hydrogen production.

2. Chemicals and reagents

The precursor of ruthenium used was ruthenium acetylacetonate (97 %) was purchased from Sigma-Aldrich and the commercial alumina (γ-Al_2O_3, $S_{BET} = 187\ m^2g^{-1}$) from Sued Chemie. Absolute ethanol (99.9 %) was acquired from Sigma-Aldrich. For the TiO_2 nanostructure synthesis a titanium foil (0.125 mm, 99.6 % purity) was purchased from Research Materials Ltd. The agents used for the anodization were: ethylene glycol (99 %) purchased from VWR, ammonium fluoride (98 %) from Sigma-Aldrich, acetic acid (99 %) from Sigma-Aldrich and 2-hydroxyethylamine (99 %) from Sigma-Aldrich. For the water splitting reaction the agent used was KOH (99.9 %) from Sigma-Aldrich.

3. Experimental section

3.1. Synthesis and characterization of ruthenium catalyst

The catalyst was synthesized by the impregnation method with ethanol and consists of Ru supported on alumina. The appropriate amount of ruthenium acetylacetonate to obtain a Ru loading of 2 wt % was mixed with ethanol until dissolved. Later, alumina was added to the solution (100 mL of ethanol per gram of support added). The mixture was placed on a hot plate stirrer at 60 °C under mild stirring in order to completely evaporate the solvent. Then, the solid was recovered and dried at 60 °C for 8 h and then calcined in static air at 500 °C for 3.5 h in a muffle furnace. The catalyst was heat-treated in a flow of H_2 at 250 °C for 1 h. The catalyst was labelled as Ru/Alum.

Ru/Alum was thoroughly characterized using different techniques. N_2 adsorption isotherms were carried out at −196 °C in a Micromeritics ASAP 2460 apparatus (Norcross, GA, USA). Prior to the analysis, the catalyst (Ru/Alum) and the support (alumina) were degassed at 150 °C. The specific surface area (S_{BET}) was determined in the relative pressure range of 0.05–0.25. X-ray diffraction (XRD) analysis was performed in order to determine the nature of the crystalline phases. The equipment used was an Enraf Nonius FR590 sealed tube diffractometer (Bruker, Delft, The Netherlands) equipped with a monochromatic Cu Kα1 source (30 mA and 40 kV). High resolution transmission electron microscopy (HRTEM) was carried out to observe the catalyst structure and morphology. A field emission gun TECNAI G2 F20 microscope (FEI Company, Hillsboro, OR, USA) at 200 kV and a JEM 3000 F microscope (JEOL, Tokyo, Japan, 300 kV) were employed. TEM images were used also to determine the ruthenium particle-size average. XPS experiments were undertaken in order to determine the characteristics of the near surface especially the oxidation state of Ru. XPS analysis was undertaken with a Kratos Axis ultra DLD photoelectron spectrometer with a non-monochromatized Mg Kα X-ray source ($h\nu = 1253.6$ eV). An analyser pass energy of 50 eV was used for survey scans and 20 eV for detailed scans. Binding energies were referenced to the C1s peak from adventitious carbonaceous considering a binding energy of 284.8 eV. A CasaXPS software for the analysis of the results. Iterations were done with the Marquardt method and following the restrictions optimized by Morgan [30].

3.2. Synthesis and characterization of TiO_2 nanostructure

The TiO_2 nanostructure was synthesized by electrochemical anodization, using a 1 × 1 cm titanium foil. Before anodization, the titanium sample was ultrasonically cleaned in acetone, ethanol and water for 2 min in each solvent and dried with nitrogen.

Anodization was performed at room temperature in an electrolyte composed of ethylene glycol, containing 1 M water, 0.05 M ammonium fluoride and 1 vol% of a mixture of acetic acid and 2-hydroxyethylamine. The sample was anodized for 30 min at 55 V, using Ti foil as the anode and platinum sheet as the cathode. Anodized Ti was rinsed with deionized water, dried in nitrogen, and then annealed at 450 °C for 1 h.

The crystalline structure of the sample was also studied by X-ray diffraction (XRD), using a Philips X'Pert diffractometer equipped with an Enraf Nonius FR590 type generator whose CuKα radiation is filtered with nickel (λ = 0.1542 nm). The nanostructure morphology was observed with a Field Emission Scanning Electron Microscope (FESEM) at an acceleration potential of 5 kV and a Transmission electron microscopy (TEM) at 200 kV.

3.3. Reaction system and analytical method

Hydrogen was produced in a three-electrode system: the TiO_2 nanostructure as the working electrode (0.5 cm^2 exposed to the electrolyte), a platinum foil as counter electrode and an Ag/AgCl (3 M KCl) electrode as the reference electrode, all of them immersed in a 1 M KOH electrolyte. A Nafion membrane was placed between anode and cathode to avoid gas crossover.

The output of the platinum cell was connected to the reactor through a metallic pipeline (1/16 inch) in order to transport the hydrogen generated and use it in the hydrogenation reaction.

A potentiostat (PalmSens4) was used to apply a constant potential of 1 $V_{Ag/AgCl}$ for 4 or 8 h depending on the reaction time, and a UV lamp (Opsytec) with a wavelength of 365 nm was used to generate the light incident on the nanostructure through a quartz window. Before starting the test, the entire system was purged with nitrogen, and leak tested. The production of pure hydrogen was checked by gas chromatography using a HP equipped with a Porapak Q column.

The hydrogenation reaction was carried out in a 25 mL two-neck flask used as a reactor. The reactor was fed with 3.5 mL of an aqueous solution of LA (0.05 M) and 0.1 g of Ru/Alum. A conduction from the three-electrode hydrogen production system, was introduced into liquid media of the reactor (Fig. 1). This reactor was placed in a silicone bath at the desired temperature for the required time. The reactor had an opening to prevent overpressure.

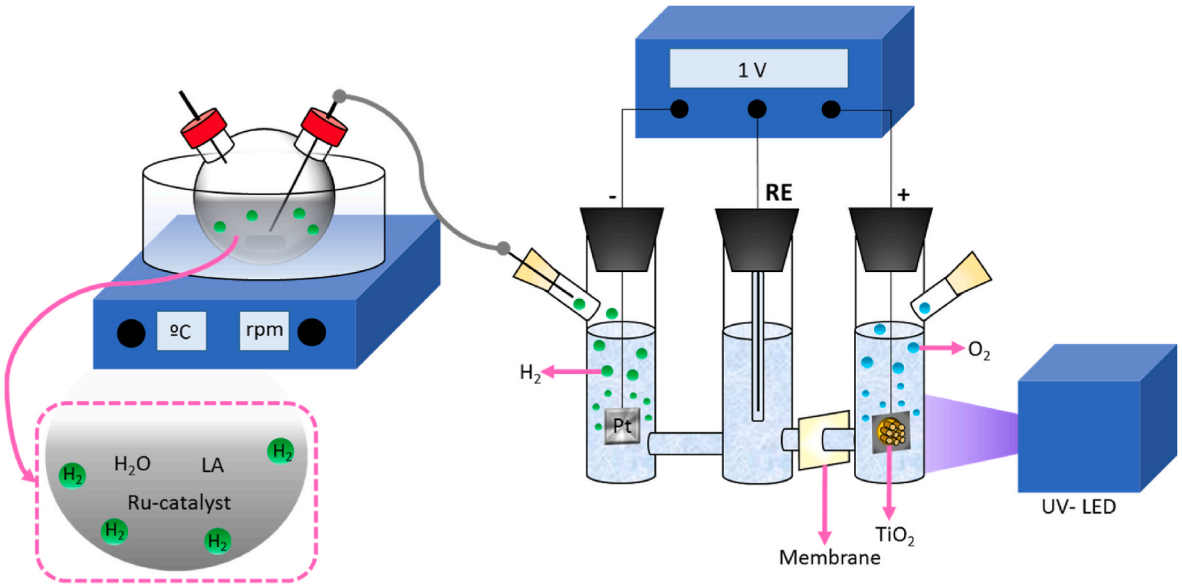

Fig. 1. Schematic diagram to produce hydrogen by photoelectrochemical water splitting with a nanostructured TiO_2 photocatalyst and its use to produce γ-valerolactone from biomass derivatives using a Ru based catalyst.

The liquid reaction products were collected by filtration in order to carry out a quantitative analysis. The reaction products and the reactants were analyzed by gas chromatography using GC equipped with a FID detector. The GC instrument employed was Hewlett Packard 5890 (Palo Alto, California, USA), equipped with an Agilent HP-1 column (30 m × 0.32 mm × 0.25 mm). The FID detector worked at 240 °C, the injection port standing at 220 °C. In a typical run, the temperature program was: (i) 35 °C isothermal for 30 min, (ii) from 35 to 230 °C with a heating rate of 1.5 °C min^{-1}, and (iii) isothermal at 230 °C for 15 min. In order to identify the reaction byproducts a gas chromatograph mass spectrometer (GC-MS) (Hewlett Packard 5890 (Palo Alto, California, USA)) was used. It was equipped with a ZB-Wax plus, Zebron column (phenomenex): 30 m × 0.25 mm × 0.25 μm. The temperature program employed for the analysis in GC-MS was the same as that used by GC-FID. For these experiments, dodecane was used as an internal pattern for quantification of the reaction products. C-balance was done comparing the decrease of the LA area with the conversion determined using dodecane as an internal pattern.

4. Results

4.1. Characterization results

Fig. 2a shows a TEM image and Fig. 2b and c shows HR-TEM images, where it can be observed that Ru nanoparticles are properly dispersed onto the alumina support. Moreover, a histogram was accomplished with the HR-TEM images (Fig. 2d) in order to estimate the average size of Ru nanoparticles, which was around 9 nm. The BET surface area was analyzed by N_2 adsorption. The surface area of the Ru/Alum catalyst was 159 m^2/g, which is slightly lower than that of the support (187 m^2/g). Fig. 2e displays the XPS characterization, which was used to know the oxidation state of the Ru species on the near surface of the catalyst. The analysis showed asymmetric peaks related to metallic Ru for both Ru 3d and Ru 3p orbitals. Binding energy values fit with the ones reported for metallic Ru (279.90 and 284.07 eV) [30], whereas no oxidized Ru species were detected. Fig. 2f presents the XRD pattern of the sample of ruthenium before and after the reduction treatment with H_2. Peaks related to ruthenium oxide at $2\theta = 28.1°$, 35.2°, 54.3° corresponding to (110), (101), (211) planes were observed in the catalyst before the reducing treatment, and they confirm the crystalline nature of the material (JCPDS 21-1172) [31]. In the sample after the treatment (Ru/Alum), the peaks related to RuO_2 were not observed. However, new peaks of low intensity related to metallic hexagonal ruthenium (JCPDS 06-0663) were detected at $2\theta = 38.1°$, 42.6°, 44.7°, 58.4° corresponding to (100), (002), (101) and (102) planes [32].

As mentioned above, the TiO_2 nanostructure used as a photocatalyst was synthesized by electrochemical anodization, using an organic electrolyte in the presence of fluorides. Fig. 3a shows the variation of current density as a function of time during anodization. The obtained curve is characteristic of the nanotubular structure formation [26,33]. Consequently, the three typical zones of titanium dioxide growth can be distinguished. The first stage (I) shows an abrupt drop in current density, due to the formation of a compact TiO_2 layer that opposes the passage of electric current. The second stage (II) presents a slight increase in current density, due to crack appearance or pitting because of the presence of fluoride ions in the electrolyte, which cause localized dissolution of the compact oxide [33,34]. Lastly, the third stage (III) shows a slight decline in current density and its stabilization in quasi-steady state, this is caused by the formation and dissolution rates of the oxide being approximately equal to each other [34]. Fig. 3b displays the X-ray diffraction results for the TiO_2 nanostructure, where main diffraction peaks characteristic of anatase TiO_2 phase can be seen at $2\theta = 25.2$; 38.2; 40.9; 48.1; 53.9; 62.2, 70.9 and 76.2° [35–37]. The anatase phase has been selected as a photoelectrocatalyst since it has been reported to present a good performance in the hydrogen production, due to the order of its crystalline structure [38,39]. On the other hand, Fig. 3c and d shows the morphological characterization of the nanostructure, using FE-SEM and TEM, respectively. Fig. 3c depicts the synthesis of smooth-walled tubular structures, with an average pore diameter and length of 43 ± 4 nm and 5.6 ± 0.6 μm, respectively. Additionally, Fig. 3d displays a representative TEM image of the TiO_2 nanostructure employed in this experiment. In order to undertake this analysis, the sample was obtained by subtly scratching the external part of the layer, which is the active oxidized material. This sample consists of tubes of variable width (from 10 to 100 nm) and length. In most cases these tubes are packed together forming non-regular compact structures. The nanotube surface is not flat but it is covered of rough entities, similar to nanoparticles adhered on the surface of the tubes. A closer look to the images reveals the clear presence of microporosity. This morphology with the joint feature of non-regular surface plus microporosity ensures the achievement of an elevated surface area. On the other hand, the measurement of the interplanar distances (see inset) of 1.70, 1.89, 2.33

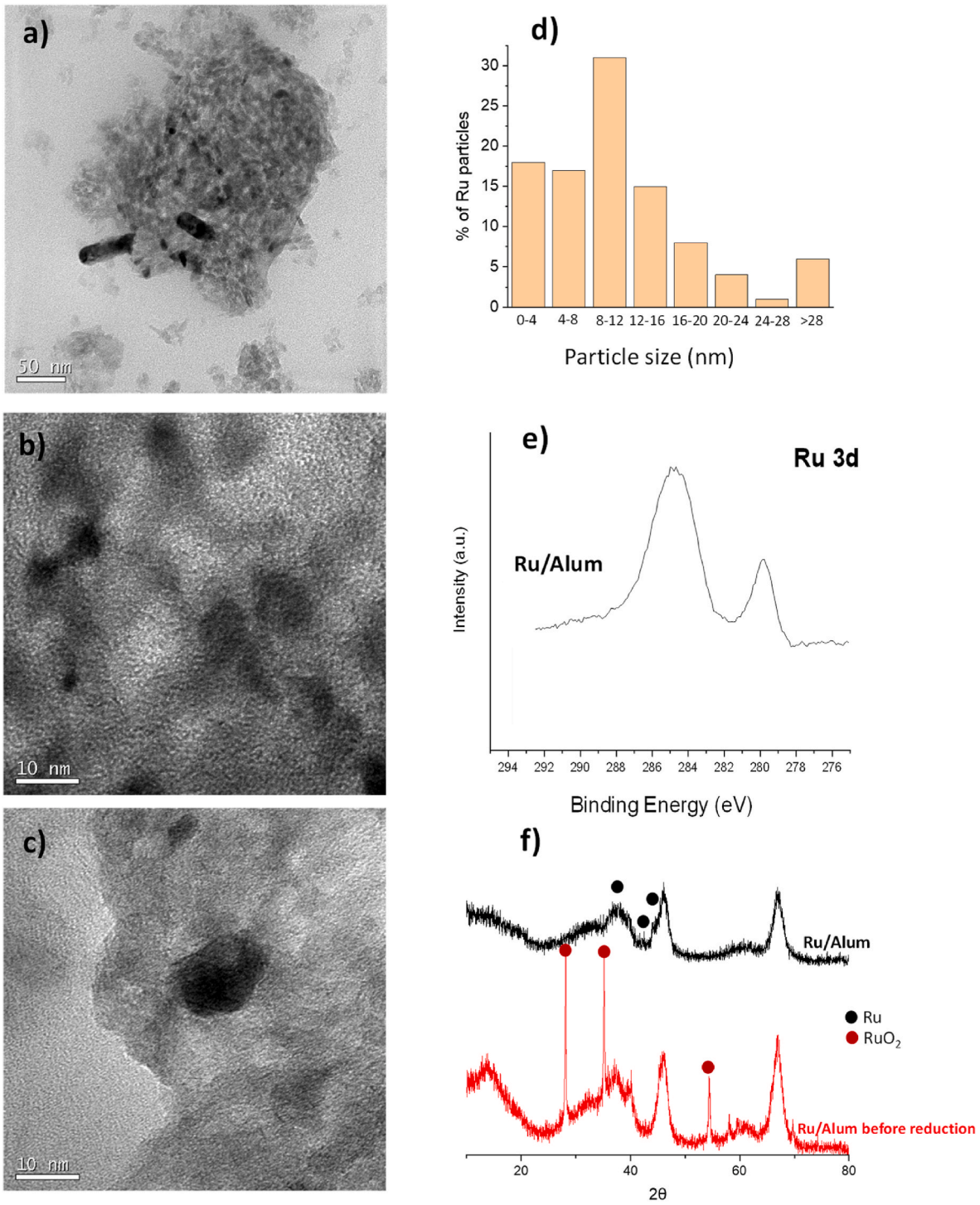

Fig. 2. Characterization of Ru/Alum by transmission electron microscopy (TEM) (a), HR-TEM (b, c), histogram of the Ru particle size (d), XPS analysis (e) and XRD (f).

and 3.52 Å confirms that tetragonal TiO_2 anatase (JCPDS: 021-1272) is the only Ti-containing phase detected. This data is in agreement with the results observed by XRD about the nature of the titanium dioxide. Fig. 3e shows the photoelectrocatalytic response of the nanostructure at 1 $V_{Ag/AgCl}$ during 8 h illuminated at $\lambda = 365$ nm. It is key to highlight that when UV light is incident on the surface of the nanostructure, the current density immediately increases to a maximum, a behavior that can be associated with internal electron-hole pairs generation and fast charge separation [40]. According to the registered results, a current density of 12.5 mA cm^{-2} was obtained, this remained constant throughout the test, which allowed determining that the synthesized nanostructure presents great stability. Additionally, it was possible to determine the number of moles and the hydrogen flow generated during the test by using Faraday's law, being in this case 0.23 mmol h^{-1} cm^{-2} and 5.70 mL h^{-1} cm^{-2}, respectively.

Table S1 displays some general parameters associated with the photoelectrochemical characterization of TiO_2. Raman spectra (Fig. 4a) show four peaks at 141.7, 396.2, 515.1 and 639.3 cm^{-1} typical of the titanium oxide in the anatase phase [37], confirming that observed by XRD. In addition, Fig. 4b shows the photoelectrochemical behavior of

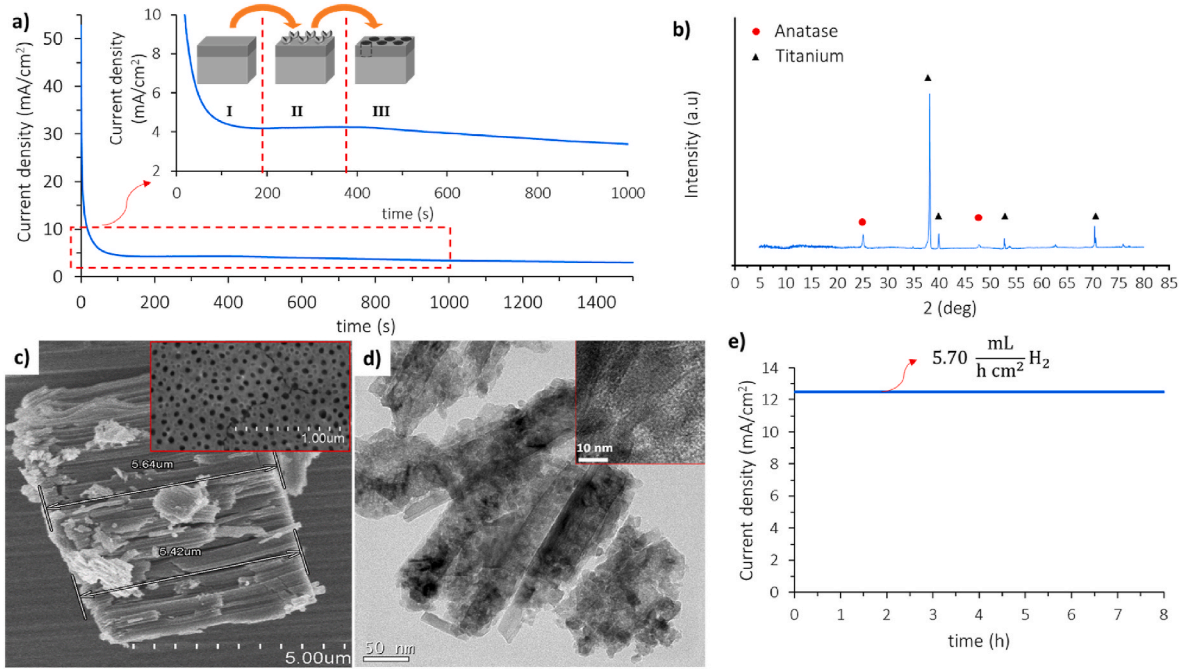

Fig. 3. Characterization of TiO_2 nanostructures. Current density transients recorded during anodization of titanium (a), XRD patterns (b), Cross-sectional and top-view FESEM images (c), TEM images (d), and photocurrent density vs time (e).

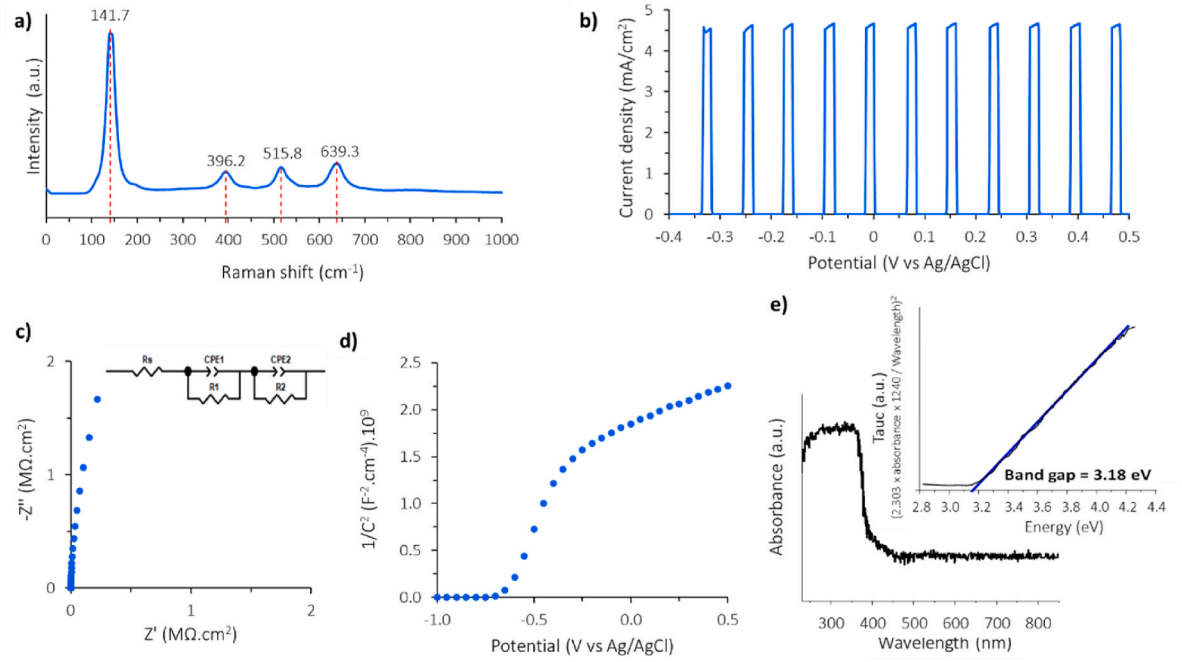

Fig. 4. Structural and photoelectrochemical characterization of TiO_2 nanostructure. Raman spectra (a). Photocurrent transient vs. potential curve (b). Nyquist plots (inset: electrical equivalent circuit used to simulate EIS results) (c). Mott-Schottky diagram (d). UV spectra (inset: Band gap energy using the Tauc plot from DR-UV-Vis) (e).

the TiO_2 nanostructure by a water splitting test. From the results attained, it is observed that high current densities are reached within the whole range of applied potential. Therefore, the analyzed TiO_2 nanostructure obtained a good photoelectrochemical behavior applying low polarization. These results agree with the electrochemical impedance spectroscopy test and the Mott-Schottky analysis (Fig. 4c and d, respectively). In the first case, with the electrochemical impedance spectroscopy test and the fitting of the system to the equivalent electrical circuit (inset of Fig. 4c), the resistance of the sample to charge transfer can be studied [41]. With the selected circuit, the sample is adjusted to a bilayer system, formed by a compact inner layer and a porous outer layer. The results obtained correspond with those reported in the literature, since the internal layer was found to be highly resistive compared to the external ($R_2 \gg R_1$) [42]. Additionally, the resistance of the external layer ($R_1 = 16.06\ \Omega\ cm^2$) is related to the high porosity and surface area of the sample, parameters that favor the photoelectrochemical performance of the nanostructure. Besides, in the Mott-Schottky diagram, a linear zone with positive slope was obtained;

therefore, the nanostructure behaves as an n-type semiconductor [43]. Through this test it was possible to determine that the charge donor density (N_D) and flat band potential (E_{FB}) are $4.95 \cdot 10^{19}$ cm^{-3} and −0.70 $V_{Ag/AgCl}$, respectively; these values correspond with what is reported in the literature and are associated with the number of defects present in the nanostructure, which facilitate charge separation and prevent recombination of the electron-hole pairs [37]. To complement the characterization of the TiO_2 nanostructure, the UV–Visible spectroscopy test and the adjustment of the data to the Tauc equation were carried out (Fig. 4e), so it was possible to determine that the band gap of the sample is 3.18 eV. Comparing this result with the literature for TiO_2 in anatase phase (3.2 eV [44]), it is possible to state that the synthesized nanostructure presents slightly better photoelectroactivity, due to the wavelengths range of the solar spectrum in which electron-hole pairs can be generated is expanded [45].

4.2. Catalytic results

As mentioned in the introduction part, ruthenium based materials are the most efficient catalysts for the LA to GVL reaction, especially if the reaction takes place in an aqueous media. For this reason, we used a ruthenium catalyst supported on γ-alumina. The catalyst synthesized, Ru/Alum, was previously tested in order to check its catalytic performance using as a hydrogenating source either pressurized hydrogen or a flow of H_2. These experiments were carried out using two different reaction temperatures (30 and 60 °C). In all cases, high yields to GVL were achieved. Using the same conditions of Table 1 but using lower LA concentration (0.05 M) conversions higher than 98 % were obtained in all the experiments. Increasing the LA concentration to 0.12 M the GVL yields were also very high (Table 1) although lower than with 0.05 M. The highest LA conversions were obtained with pressurized hydrogen (30 bar). We must indicate that, with this ruthenium catalyst, the selectivity to GVL was always higher than 90 % in all the experiments conducted (Table 1).

As we could confirm that this Ru-catalyst is efficient for the hydrogenation of levulinic acid into γ-valerolactone, then we proceeded to use our coupled system employing the TiO_2 nanostructure to get hydrogen from water and then, the ruthenium catalyst to hydrogenate the levulinic acid. Before this, two preliminary experiments were carried out using the coupled system (Fig. 1). In a first assay, the TiO_2 nanostructure was used to produce hydrogen from water but no Ru-catalyst was present. In this case, no LA conversion was observed since hydrogen was produced but the catalytic sites that allows the LA to GVL reaction were absent. In a second test, the Ru/Alum catalyst was used but the TiO_2 nanostructure was not added to the cell. In this case, very low LA conversions were observed (<0.2 %) and only traces of GVL could be appreciated. This negligible LA transformation is due to the lack of hydrogen in the media as the TiO_2 nanostructure was absent in the cell.

Interestingly, the joint use of the TiO_2 nanostructure and the Ru catalyst led to a drastic positive variation, with a substantial GVL formation. Fig. 5 (and Table 2) shows the results of the transformation of LA into GVL using the hydrogen produced in the photoelectrochemical cell from water splitting with the TiO_2 photocatalyst and the Ru-based catalyst.

Table 1
Transformation of LA into GVL using 2Ru/Alum using pressurized hydrogen or flowing hydrogen. Reaction conditions: LA (0.12 M), H_2 (30 bar or 100 mL/min) and reaction time of 2 h.

Temperature (°C)	H_2	LA conversion (%)	Yield to GVL (%)	Selectivity to GVL (%)
30	30 bar	90.0	83.0	92.2
	flow	33.2	30.3	91.2
60	30 bar	95.9	88.1	91.9
	flow	95.4	90.2	94.6

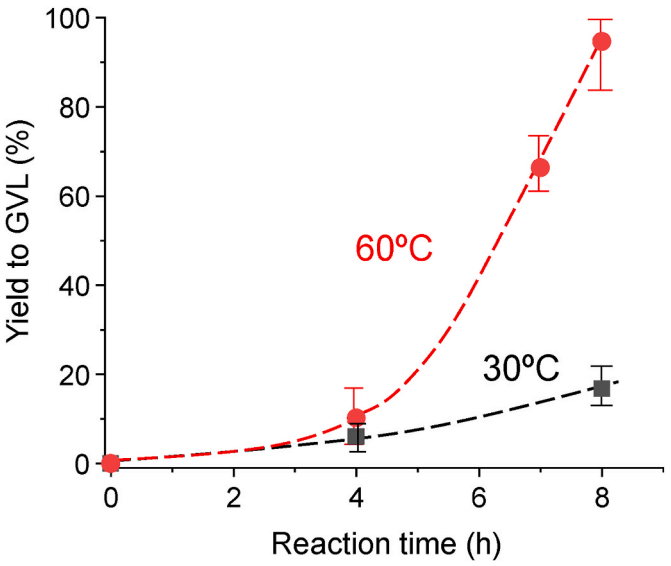

Fig. 5. Influence of the reaction time on the GVL yield in the LA to GVL reaction using the coupled system at 30 (■) and 60 °C (●). Note: Ru/Alum (biomass hydrogenation) and nanotubes of TiO_2 (hydrogen production) have been used. Remaining reaction conditions in text.

Table 2
Transformation of LA into GVL using hydrogen from photoelectrochemical water splitting.

Temperature (°C)	Reaction time (h)	LA conversion (%)	Yield to GVL (%)	Selectivity to GVL (%)	C-balance (%)
60	8	98.0	94.6	96.5	100
	7	70.2	66.3	94.4	97
	4	17.0	10.2	60.0	91
30	8	25.7	16.8	65.4	95
	4	10.2	6.9	67.6	90

Reaction conditions: 3.5 mL of an aqueous solution of LA (0.05 M) and 0.1 g of Ru/Alum. Using hydrogen gas, which was produced by photoelectrochemical water splitting using a TiO_2 nanostructure.

It can be observed that at 30 °C the conversion of LA was ca. 10 % after 4 h of reaction and the yield to GVL was close to 7 %. The conversion of LA increased until ca. 26 % after 8 h of reaction and the yield to GVL achieved ca. 17 %. In these tests, the selectivity to GVL was ca. 66 %. As expected, when the reaction was carried out at 60 °C, the LA conversion and the yield to GVL increased. Then, after a reaction time of 7 h, LA conversion of 70 % and a yield to GVL of ca. 66 % were achieved. If the reaction time increases until 8 h of reaction the LA conversion was almost total and the yield to GVL achieved was 94.6 %. When the reaction temperature was increased from 30 to 60 °C, the selectivity to GVL significantly improved. We must indicate that other byproducts (identified by GC-MS) were detected in low quantities (Fig. S1).

The theoretical production of hydrogen was calculated to be 0.116 mmol h^{-1}. Considering that there were 0.175 mmol of LA in each catalytic reaction to achieve a theoretical conversion of 100 % of LA, it would be necessary at least 1.5 h of reaction. After 7 h of reaction a yield to GVL of 66.3 % was achieved, which means 14.3 % of efficiency in the use of the produced hydrogen by water splitting and after 8 h of reaction a 17.7 % of the H_2 produced was consumed to produce GVL from LA.

The low conversion of LA at short reaction times (i.e. 4 h) is due to the period of time required for the displacement of nitrogen through the electrochemical cell and the time which takes to increase the concentration of hydrogen in the head space and is able to reach the catalytic reactor through the line joining both systems. Hence, a certain time is

necessary for hydrogen to fully reach the catalytic reactor. Therefore, lower conversions of LA were obtained at short reaction times while increased significantly after a certain time.

In addition, it is important to note that the nanostructure used as a photocatalyst allows obtaining hydrogen in a reproducible and stable way. In fact, it was confirmed that TiO_2 nanotubes can be reused for at least 20 tests without affecting its photoelectrocatalytic properties. This stable performance of the TiO_2 nanostructure was further confirmed using this nanostructure to produce hydrogen for 5 catalytic cycles, employing new levulinic acid with Ru-catalyst to produce the hydrogenation (Fig. 6), this way, confirming its extremely good stability.

At this point, we have checked the stability of the nanostructure that generates hydrogen. However, we do not know the stability of the catalyst. Accordingly, new experiments have been undertaken using the same catalyst after filtering it from the aqueous media and drying. Unfortunately, the catalytic activity drastically fell from ca. 70 % until12 % (Fig. S2). In order to see if this fall was related to the undesired oxidation of the catalyst, a reduction in H_2 flow at 250 °C for 1 h was carried out. Then, this regenerated catalyst was tested again in the LA hydrogenation. Interestingly, the LA conversion and the yield to GVL were maintained at the same level. A third run was also undertaken, leading also to similar values (even a slight increase in activity was observed).

As a summary, in the present work, it has been shown for the first time that a coupled system (photoelectrocatalytic water splitting and transformation of LA) can obtain a yield to GVL of 94 % at a temperature of 60 °C and at ambient pressure. Through this article we have demonstrated that it is possible to store the hydrogen produced from water transforming a biomass derivative compound into a versatile fuel precursor which, conversely to hydrogen, can be easily stored and handled.

5. Conclusions

For the first time a coupled system involving H_2 production from water by photoelectrocatalysis and a catalytic biomass valorization reactor has been successfully developed, achieving outstanding yields to γ-valerolactone at ambient pressure and low temperatures. As this reaction can take place at low temperature, the energy necessary is very low, which makes more economical and sustainable a possible applied process.

In this sense, the synthesized TiO_2 nanostructure was possible to produce, by photoelectrochemical process, the necessary amount of hydrogen to transform levulinic acid into γ-valerolactone using a ruthenium-based catalyst. The water splitting process for hydrogen production was carried out in a stable and reproducible way, since the nanostructure used presented high stability even after several 20 reuses. The catalyst was also shown to be highly stable whenever a reductive regeneration was undertaken. Without that reductive regeneration, the catalyst showed a poor performance.

This innovative system was able to achieve more than 94 % of yield to γ-valerolactone with an efficiency of hydrogen higher than 17 % after 8 h of reaction under mild conditions. The results prove that hydrogen produced by photoelectrochemical water splitting can be a suitable hydrogen source to directly carry out hydrogenation reactions.

Moreover, it has been demonstrated that it is possible to store the hydrogen in the form of γ-valerolactone, which, in contrast with hydrogen, can be transported and stored in a relatively easy way. These results are truly promising; however, it should be noted that further improvements could be done. For example, the water splitting could be undertaken using solar light instead of UV light. Moreover, the Ru-catalyst could be also optimized in order to obtain higher yields to GVL at temperatures lower than 60 °C optimizing the catalysts. These two improvements could help to facilitate and economize the process.

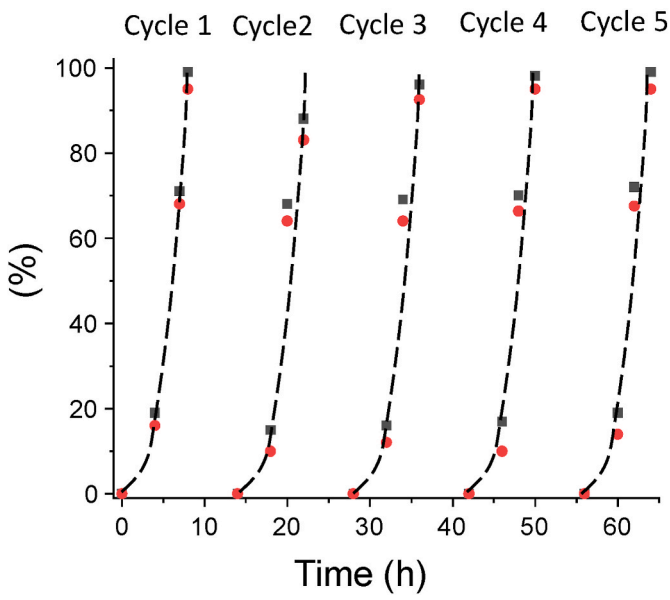

Fig. 6. Stability of the TiO_2 nanostructure used for hydrogen production and further LA to GVL transformation using the coupled system. Symbols: LA conversion (■) and Yield to GVL (●). Note: Ru/Alum (biomass hydrogenation) and nanotubes of TiO_2 (hydrogen production) have been used. Reaction temperature of 60 °C. Remaining reaction conditions in text.

CRediT authorship contribution statement

Adrián García: Investigation, Validation, Writing – original draft. **Elianny Da Silva:** Investigation, Methodology, Validation. **María Erans:** Formal analysis, Methodology. **Ramón Fernández-Domene:** Data curation, Formal analysis, Validation. **Rita Sánchez-Tovar:** Conceptualization, Funding acquisition, Supervision, Writing – review & editing. **Benjamin Solsona:** Conceptualization, Supervision, Writing – review & editing, Funding acquisition.

Data availability

Data will be made available on request.

Acknowledgements

M.E. is grateful for Grant RYC2021-031428-I funded by MCIN/AEI/10.13039/501100011033 and by European Union NextGenerationEU/PRTR. Authors would like to acknowledge the Generalitat Valenciana for CIAICO/2021/094, CIGRIS/2022/198 and CIGE/2022/166. A.G. thanks MINECO is acknowledged for the A.G. grant (PRE2018-085211) and the project PID2021-1262350B-C33. Thanks to SCSIE-UV for assistance in characterization of materials.

Appendix A. Supplementary data

Supplementary data to this article can be found online at https://doi.org/10.1016/j.biombioe.2023.107020.

References

[1] J.P. Lange, Catalysis for biorefineries–performance criteria for industrial operation, Catal. Sci. Technol. 6 (2016) 4759–4767.
[2] P. Lanzafame, G. Centi, S. Perathoner, Evolving scenarios for biorefineries and the impact on catalysis, Catal. Today 234 (2014) 2–12.
[3] A.A. Arpia, W.H. Chen, S.S. Lam, P. Rousset, M.D.G. De Luna, Sustainable biofuel and bioenergy production from biomass waste residues using microwave-assisted heating: a comprehensive review, Chem. Eng. J. 403 (2021), 126233.

[4] M. Choi, J. Byun, H. Park, K. Jeong, S.M. Kim, J. Han, Economically-feasible "greener" transformation of gamma-valerolactone to nylon 6,6, Biomass Bioenergy 162 (2022), 106503.

[5] C. Moustani, E. Anagnostopoulou, K. Krommyda, C. Panopoulou, K.G. Koukoulakis, E.B. Bakeas, G. Papadogianakis, Novel aqueous-phase hydrogenation reaction of the key biorefinery platform chemical levulinic acid into γ-valerolactone employing highly active, selective and stable water-soluble ruthenium catalysts modified with nitrogen-containing ligands, Appl. Catal., B 238 (2018) 82–92.

[6] M.J. Climent, A. Corma, S. Iborra, Conversion of biomass platform molecules into fuel additives and liquid hydrocarbon fuels, Green Chem. 16 (2014) 516–547.

[7] O. Oyola-Rivera, A.M. González-Rosario, N. Cardona-Martínez, Catalytic production of sugars and lignin from agricultural residues using dilute sulfuric acid in γ-valerolactone, Biomass Bioenergy 119 (2018) 284–292.

[8] K. Yan, Y. Yang, J. Chai, Y. Lu, Catalytic reactions of gamma-valerolactone: a platform to fuels and value-added chemicals, Appl. Catal., B 179 (2015) 292–304.

[9] D.M. Alonso, S.G. Wettstein, J.A. Dumesic, Gamma-valerolactone, a sustainable platform molecule derived from lignocellulosic biomass, Green Chem. 15 (2013) 584–595.

[10] A. García, P.J. Miguel, A. Ventimiglia, N. Dimitratos, B. Solsona, Optimization of the Zr-loading on siliceous support catalysts leads to a suitable Lewis/Brønsted acid sites ratio to produce high yields to γ-valerolactone from furfural in one-pot, Fuel 324 (2022), 124549.

[11] S. Burlawar, D.J. Klingenberg, T.W. Root, C.T. Scott, C.J. Houtman, K.J. Bourne, R. Gleisner, V. Subramaniam, Effect of temperature on the rheology of concentrated suspensions containing lignocellulosic biomass particles, Biomass Bioenergy 156 (2022), 106298.

[12] A. García, E. Monti, A. Ventimiglia, N. Dimitratos, P.J. Miguel, M.L. López, I. Álvarez-Serrano, T. García, M.P. Pico, A.M. Dejoz, B. Solsona, Zr supported on non-acidic sepiolite for the efficient one-pot transformation of furfural into γ-valerolactone, Biomass Bioenergy 170 (2023), 106730.

[13] Y. Shao, S. Ba, K. Sun, G. Gao, M. Fan, J. Wang, H. Fan, L. Zhand, X. Hu, Selective production of γ-valerolactone or 1, 4-pentanediol from levulinic acid/esters over Co-based catalyst: importance of the synergy of hydrogenation sites and acidic sites, Chem. Eng. J. 429 (2022), 132433.

[14] K. Yan, A. Chen, Selective hydrogenation of furfural and levulinic acid to biofuels on the ecofriendly Cu–Fe catalyst, Fuel 115 (2014) 101–108.

[15] S.A. Sorokina, S.P. Mikhailov, N.V. Kuchkina, A.V. Bykov, A.L. Vasiliev, M. G. Ezernitskaya, A.L. Golovin, L.Z. Nikoshvili, M.G. Sulman, Z.B. Shifrina, Ru@ hyperbranched polymer for hydrogenation of levulinic acid to gamma-valerolactone: the role of the catalyst support, Int. J. Mol. Sci. 23 (2022) 799.

[16] J. Patel, A. Patel, Solvent free hydrogenation of levulinic acid over in-situ generated Ni (0) stabilized by supported phosphomolybdic acid using formic acid as an internal hydrogen source, Renew. Energy 201 (2022) 190–201.

[17] J. Gu, J. Zhang, Y. Wang, D. Li, H. Huang, H. Yuan, Y. Chen, Efficient transfer hydrogenation of biomass derived furfural and levulinic acid via magnetic zirconium nanoparticles: experimental and kinetic study, Ind. Crops Prod. 145 (2020), 112133.

[18] F.R. Malik, H.B. Yuan, J.C. Moran y N. Tippayawong, Overview of hydrogen production technologies for fuel cell utilization, Eng. Sci. Technol. 43 (2023), 101452.

[19] C.A. Grimes, O.K. Varghese, y S. Ranjan, Light, Water, Hydrogen: the Solar Generation of Hydrogen by Water Photoelectrolysis, Springer, New York, 2008.

[20] R. Van de Krol, y M. Grätzel, Photoelectrochemical Hydrogen Production, Springer, New York, 2012.

[21] J. Delgado, W.N.V. Salcedo, G. Bronzetti, V.C. Moreno, M. Mignot, J. Legros, C. Held, H. Grénman, S. Leveneur, Kinetic model assessment for the synthesis of γ-valerolactone from n-butyl levulinate and levulinic acid hydrogenation over the synergy effect of dual catalysts Ru/C and Amberlite IR-120, Chem. Eng. J. 430 (2022), 133053.

[22] A. García, P.J. Miguel, M.P. Pico, I. Álvarez-Serrano, M.L. López, T. García, B. Solsona, γ-valerolactone from levulinic acid and its esters: substrate and reaction media determine the optimal catalyst, Appl. Catal., A 623 (2021), 118276.

[23] N.T. Sahrin, R. Nawaz, F.K. Chong, S.L. Lee, M.D.H. Wirzal, Current perspectives of anodized TiO_2 nanotubes towards photodegradation of formaldehyde: a short review, Environ. Technol. Innov. 22 (2021), 101418.

[24] A. Fujishima, T.N. Rao, D.A. Tryk, Titanium dioxide photocatalysis, J. Photochem. Photobiol. C Photochem. Rev. 1 (2000) 1–21.

[25] Y. Fu, A. Mo, A review on the electrochemically self-organized titania nanotube arrays: synthesis, modifications, and biomedical applications, Nanoscale Res. Lett. 13 (2018) 187.

[26] P. Roy, S. Berger, P. Schmuki, TiO_2 nanotubes: synthesis and applications, Angew. Chem. Int. Ed. 50 (2011) 2904–2939.

[27] R.K. Karn, O.N. Srivastava, On the synthesis of nanostructured TiO_2 anatase phase and the development of the photoelectrochemical solar cell, Int. J. Hydrogen Energy 24 (1999) 27–35.

[28] Y. Xia, P. Yang, Y. Sun, Y. Wu, B. Mayers, B. Gates, Y. Yin, F. Kim, H. Yan, One-dimensional nanostructures: synthesis, characterization, and applications, Adv. Mater. 15 (2003) 353–389.

[29] M. Nischk, P. Mazierski, Z. Wei, K. Siuzdak, N.A. Kouame, E. Kowalska, H. Remita, A. Zaleska-Medynska, Enhanced photocatalytic, electrochemical and photoelectrochemical properties of TiO_2 nanotubes arrays modified with Cu, AgCu and Bi nanoparticles obtained via radiolytic reduction, Appl. Surf. Sci. 387 (2016) 89–102.

[30] D.J. Morgan, Resolving ruthenium: XPS studies of common ruthenium materials, Surf. Interface Anal. 47 (2015) 1072–1079.

[31] B. Nisha, Y. Vidyalakshmi, S.A. Razack, Enhanced formation of ruthenium oxide nanoparticles through green synthesis for highly efficient supercapacitor applications, Adv. Powder Technol. 31 (2020) 1001–1006.

[32] K.M. Eblagon, S.E. Tsang, Structure-reactivity relationship in catalytic hydrogenation of heterocyclic compounds over ruthenium black-part A: effect of substitution of pyrrole ring and side chain in N-heterocycles, Appl. Catal., B 160 (2014) 22–34.

[33] J.M. Macak, H. Tsuchiya, A. Ghicov, K. Yasuda, R. Hahn, S. Bauer, P. Schmuki, TiO_2 nanotubes: self-organized electrochemical formation, properties and applications, Curr. Opin. Solid State Mater. Sci. 11 (2007) 3–18.

[34] O. Zakir, R. Idouhli, M. Elyaagoubi, M. Khadiri, A. Aityoub, Y. Koumya, S. Rafwah, A. Abouelfida, A. Outzourhit, Fabrication of TiO_2 nanotube by electrochemical anodization: toward photocatalytic application, J. Nanomater. 2020 (2020) 1–11.

[35] A. Pancielejko, P. Mazierski, W. Lisowski, A. Zaleska-Medynska, J. Łuczak, Ordered TiO_2 nanotubes with improved photoactivity through self-organizing anodization with the addition of an ionic liquid: effects of the preparation conditions, ACS Sustain. Chem. Eng. 7 (2019) 15585–15596.

[36] J.Y. Zhang, I.W. Boyd, B.J. O'Sullivan, P.K. Hurley, P.V. Kelly, J.P. Senateur, Nanocrystalline TiO_2 films studied by optical, XRD and FTIR spectroscopy, J. Non-Cryst. Solids 303 (2002) 134–138.

[37] J. Borràs-Ferrís, R. Sánchez-Tovar, E. Blasco-Tamarit, R.M. Fernández-Domene, y J. García-Antón, Effect of Reynolds number and lithium cation insertion on titanium anodization, Electrochim. Acta 196 (2016) 24–32.

[38] T. Luttrell, S. Halpegamage, J. Tao, A. Kramer, E. Sutter, M. Batzill, Why is anatase a better photocatalyst than rutile? - model studies on epitaxial TiO_2 films, Sci. Rep. 4 (2014).

[39] W.J. Ong, L.L. Tan, S.P. Chai, S.T. Yong, A.R. Mohamed, Highly reactive {001} facets of TiO_2-based composites: synthesis, formation mechanism and characterization, Nanoscale 6 (2014) 1946–2008.

[40] C.W. Lai, S. Sreekantan, Preparation of hybrid WO_3–TiO_2 nanotube photoelectrodes using anodization and wet impregnation: improved water-splitting hydrogen generation performance, Int. J. Hydrogen Energy 38 (2013) 2156–2166.

[41] P. Xiao, B.B. Garcia, Q. Guo, D. Liu, G. Cao, TiO_2 nanotube arrays fabricated by anodization in different electrolytes for biosensing, Electrochem. Commun. 9 (9) (2007) 2441–2447.

[42] D.P. Oyarzún, R. Córdova, O.E. Linarez Pérez, E. Muñoz, R. Henríquez, M. López Teijelo, y H. Gómez, Morphological, electrochemical and photoelectrochemical characterization of nanotubular TiO_2 synthetized electrochemically from different electrolytes, J. Solid State Electrochem. 15 (2011) 2265–2275.

[43] N.B. Hakiki, S. Boudin, B. Rondot, M.D. Cunha Belo, The electronic structure of passive films formed on stainless steels, Corrosion Sci. 37 (11) (1995) 1809–1822.

[44] S. Valencia, J.M. Marín, y G. Restrepo, Bentham open open access study of the bandgap of synthesized titanium dioxide nanoparticules using the sol-gel method and a hydrothermal treatment, Open Mater. Sci. J. 9 (2010) 9–14.

[45] M. Ikram, M. Rashid, A. Haider, S. Naz, J. Haider, A. Raza, M.T. Ansar, M. Kashif Uddin, N.M. Ali, S.S. Ahmed, M. Imran, S. Dilpazir, Q. Khan, y M. Maqbool, A review of photocatalytic characterization, and environmental cleaning, of metal oxide nanostructured materials, Sustain. Mater. Technol. 30 (2021), e00343.